Interferometry in the near-infrared:
1 mas resolution at the wavelength of 1 micron

G. Weigelt[(1)], Y. Balega[(2)], T. Beckert[(1)], T. Driebe[(1)], K.-H. Hofmann[(1)], K. Ohnaka[(1)], T. Preibisch[(1)], D. Schertl[(1)], K. Smith[(1)], M. Wittkowski[(3)]

(1) MPI für Radioastronomie; (2) Special Astrophysical Observatory, Russia; (3) European Southern Observatory

Introduction

High-resolution interferometric imaging at optical and infrared wavelengths provides unique information for the study of many different classes of astronomical objects. A large number of key objects have been resolved with unprecedented resolution using bispectrum speckle interferometry or infrared long-baseline interferometry. We have studied young stellar objects (e.g., infrared counterparts of bipolar CO outflows or dust at the sublimation radius), stars at late evolutionary stages, as well as active galactic nuclei. The combination of interferometry and radiative transfer modeling enabled quantitative physical interpretations of the observations. The ESO Very Large Telescope Interferometer with its AMBER phase-closure instrument will allow us to achieve the spectacular resolution of 1 mas at the wavelength of 1 micron. The high-precision determination of small differences between visibilities at different wavelengths achievable with AMBER will very likely allow even the interferometric detection of extra-solar planets as well as the resolution of the Broad-Line Region of AGN in the infrared-wavelength region. In this poster we present a few examples of bispectrum speckle interferometry and infrared long-baseline interferometry.

VLTI VINCI interferometry of the Mira star Omicron Ceti

The observations (Fig. 1) were carried out between October 2001 and January 2003. Rosseland angular radii are derived from the measured K-band visibilities by fitting theoretical visibility functions obtained from center-to-limb intensity variations (CLVs) of Mira star models (Bessell-Scholz-Wood models). Using the derived Rosseland angular radii and the SEDs, we find effective temperatures ranging from $T_{\rm eff} = 3192 \pm 200$ K at phase $\Phi = 0.13$ to 2918 ± 183 K at $\Phi = 0.26$. Comparison of these Rosseland radii, effective temperatures, and the shape of the observed visibility functions with model predictions suggests that o Cet is a fundamental mode pulsator. Furthermore, we investigated the variation of visibility function and diameter with phase. The Rosseland angular diameter of o Cet increased from 28.9 ± 0.3 mas (corresponding to a Rosseland radius of $332 \pm 38\ R_\odot$ for a distance of $D = 107 \pm 12$ pc) at $\Phi = 0.13$ to 34.9 ± 0.4 mas ($402 \pm 46\ R_\odot$) at $\Phi = 0.4$ (see Woodruff et al. *astro-ph/0404248* for more details).

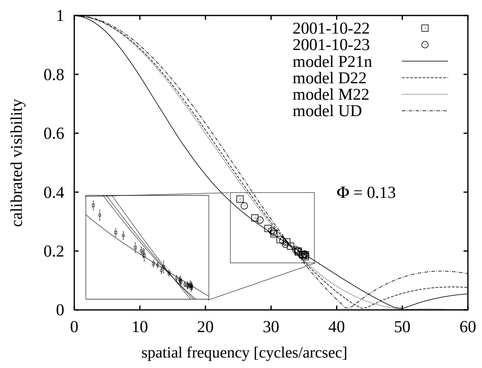

Figure 1: Visibilities of o Cet vs. spatial frequency measured at phase 0.13. The fits with different Mira star models are shown, too. Solid line represents the P model.

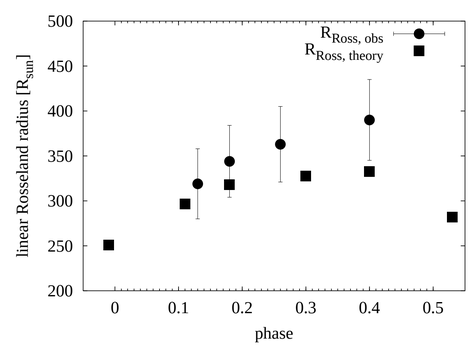

Figure 2: Observed linear Rosseland radii of o Cet derived at four different phases (filled circles) and theoretical models (filled squares). The diagram clearly shows a monotonic increase of radius with decreasing brightness, in line with the theoretical predictions.

K-band bispectrum speckle interferometry of the outflow from the massive protostellar object AFGL 2591

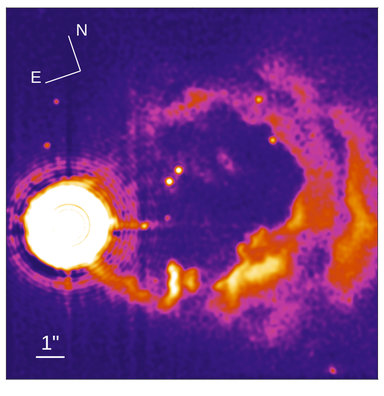

Figure 3: Pseudocolor representation of the K-band image of AFGL 2591, reconstructed using the bispectrum speckle interferometry method. In order to show the faint loop-like structures with good contrast, the intensity scale only covers intensities up to 0.2% of the peak. The bright source is not saturated. Since it is much brighter than the other features in the image (8.6 mag brighter than the star 5" north of it), it is surrounded by prominent wings.

Our reconstructed image (Fig. 3) of the outflow cavity of AFGL 2591 has a resolution of 170 mas, corresponding to physical scales of 170 AU, and shows two loops west of the compact source in unprecedented detail. The central source is clearly resolved (Fig. 4) and has a uniform-disk diameter of 40 mas (40 AU). We used 2D radiation transfer simulations to show that the resolved structure corresponds to the inner rim of a geometrically thick circumstellar disk or envelope at the dust sublimation radius (see Preibisch et al. 2003, A&A 412, pp. 735 for more details).

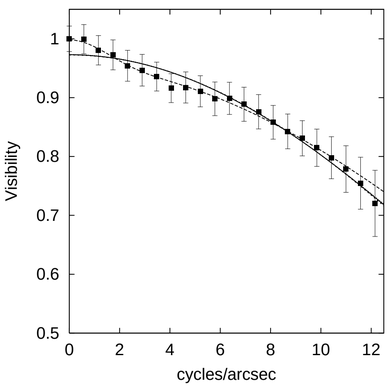

Figure 4: Radial dependence of the azimuthally averaged K-band visibility of AFGL 2591. The plot also contains several model visibilities. The visibility predicted by our radiation transfer simulation is shown as a solid line.

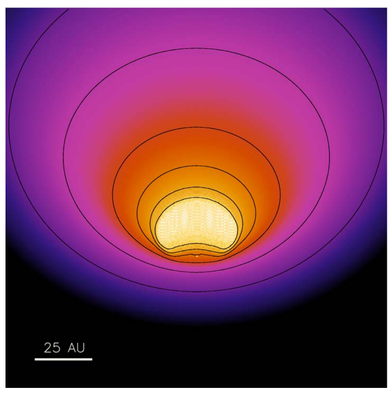

Figure 5: K-band cavity model image resulting from the radiation transfer simulations for an inclination angle of i = 30 degree. The bright white/yellow structure is the inner wall of the dusty torus-like structure at the dust sublimation radius.

Bispectrum speckle interferometry of the Seyfert 2 galaxy NGC 1068

A diffraction-limited K'-band image with 74 mas resolution and the first H-band image with 57 mas resolution were reconstructed from speckle interferograms obtained with the SAO 6 m telescope. The resolved structure consists of a compact core and an extended northern and south-eastern component. The compact core has a north-western, tail-shaped extension as well as a fainter, south-eastern extension. The K'-band FWHM diameter of this resolved compact core is $\sim 18 \times 39$ mas or 1.3×2.8 pc (FWHM of a single-component Gaussian fit; fit range 30–80% of the telescope cut-off frequency; the diameter errors are ± 4 mas), and the position angle (P.A.) of the north-western extension is $-16 \pm 4°$. If 40% of the flux from the compact K' core is emission from a point source and 60% from a Gaussian intensity distribution, then a slightly larger FWHM of approximately 26×58 mas is obtained for the compact K' component. In the H band, the FWHM diameter of the compact core is approximately 18×45 mas (± 4 mas), and the P.A. is $-18 \pm 4°$. The extended northern component (P.A. $\sim 0°$) has an elongated structure with a length of about 400 mas or 29 pc. The P.A. of $-16 \pm 4°$ of the compact 18×39 mas core is very similar to that of the western wall (P.A. $\sim -15°$) of the bright region of the ionization cone. This suggests that the H- and K'-band emission from the compact core is both thermal emission and scattered light from dust near the western wall of a low-density, conical cavity or from the innermost region of a parsec-scale dusty torus heated by the central source (the dust sublimation radius of NGC 1068 is approximately 0.1 – 1 pc). The northern extended 400 mas structure lies near the western wall of the ionization cone and coincides with the inner radio jet (P.A. $\sim 11°$). The large distance from the core suggests that the K'-band emission of the northern extended component is scattered light from the western cavity region and the radio jet region.

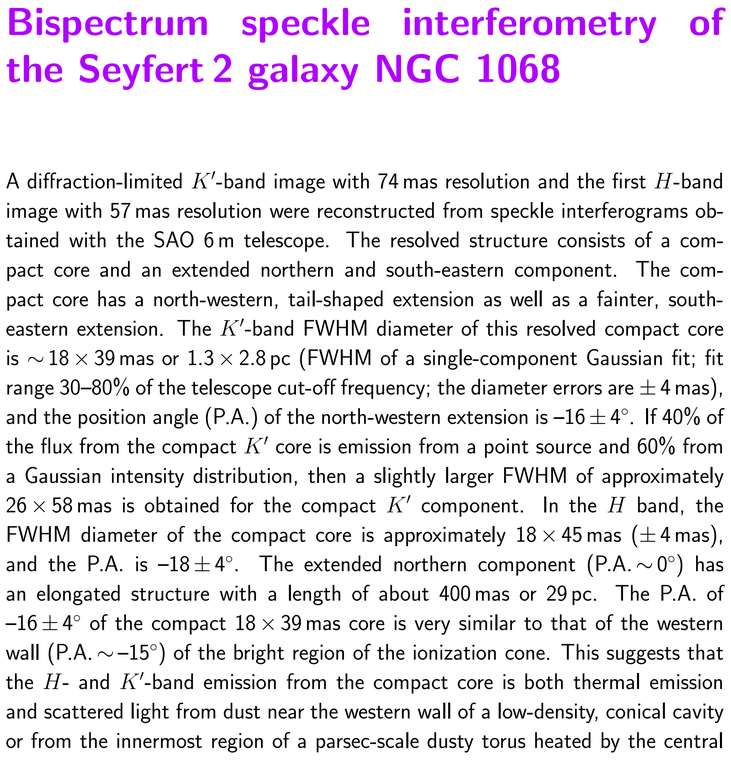

Figure 6a: Diffraction-limited K'-band image of NGC 1068 reconstructed by bispectrum speckle interferometry. The image shows the compact core (yellow) with its tail-shaped, north-western extension at a P.A. of $\sim -16°$ as well as the northern and south-eastern extended components (red). In addition to these structures, the first diffraction ring around the compact component is visible. North is up, and east is to the left. **Right, top, and bottom:** Diffraction-limited H-band image, which also shows the tail-shaped, north-western extension.

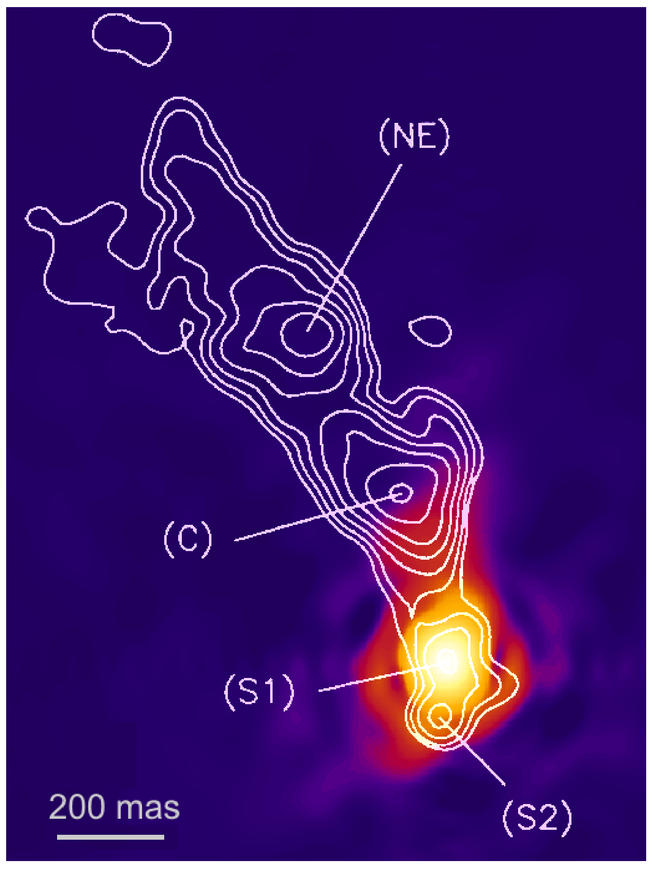

Figure 6b: MERLIN 5 GHz contour map (Gallimore et al. 1996, ApJ 464, pp. 198) superposed on our K' image. The center of the radio component S1 coincides with the center of the K' peak. The P.A. of –16° of the 18×39 mas K'-band core is very similar to that of the western wall (P.A. $\sim$–15°) of the bright region of the ionization cone. The northern extended 400 mas structure (red) aligns with the direction of the inner radio jet (S1 – C). The northern borderline of the northern component is almost perpendicular to the radio jet between C and NE. The P.A. of the south-eastern extended component is similar to the P.A. of S1 – S2.

VLTI long-baseline interferometry of NGC 1068

The first near-infrared K-band long-baseline interferometry of the nucleus of NGC 1068 with resolution $\lambda/B \sim 10$ mas was obtained with the Very Large Telescope Interferometer (VLTI; two 8.2 m diameter telescopes UT 2 and UT 3). The adaptive optics system MACAO was employed to deliver wavefront-corrected beams to the K-band instrument VINCI. A squared visibility amplitude of 16.3 ± 4.3 % was measured for NGC 1068 at a sky-projected baseline length of 45.8 m and azimuth angle 44.9 deg. This value corresponds to a FWHM size of the observed K-band structure of 5.0 ± 0.5 mas (0.4 ± 0.04 pc) if it consists of a single Gaussian component. Taking into account K-band speckle interferometry observations (Wittkowski et al. 1998, A&A 329, pp. L45; Weinberger et al. 1999, AJ 117, pp. 2748; Weigelt et al., A&A accepted), we favor a multi-component model for the intensity distribution, where one part of the flux originates from scales clearly smaller than ~ 5 mas ($\lesssim 0.4$ pc) and another part from larger scales. The K-band emission from the small ($\lesssim 5$ mas) scales might arise from the substructure of the dusty torus or directly from the central accretion flow viewed through only moderate extinction (see Wittkowski et al. 2004, A&A 418, pp. L39 for more details).

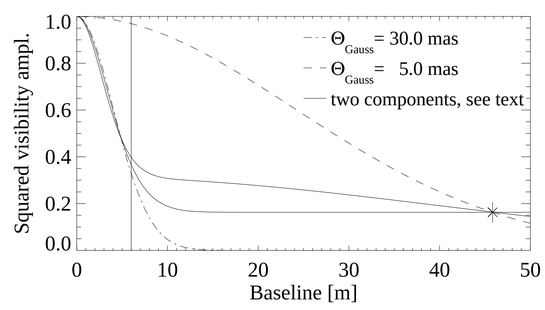

Figure 7: Synthetic squared visibility function for (dashed line) a 5 mas Gaussian, (dashed-dotted line) a 30 mas Gaussian, and (solid lines) two examples of a two-component model where (upper line/ lower line) 56%/ 40% of the total flux comes from a 3 mas/ 0.1 mas Gaussian and the remaining 44%/ 60% from a 54 mas/ 42 mas Gaussian (FWHM). Measurements are available for baselines $B = 46$ m and up to $B = 6 - 10$ m as discussed above. Both measurements are only matched if the small component has a size clearly below ~ 5 mas and if only part of the total flux in our FOV arises from this $\lesssim 5$ mas component and another part from a larger component.

Clumpy torus model

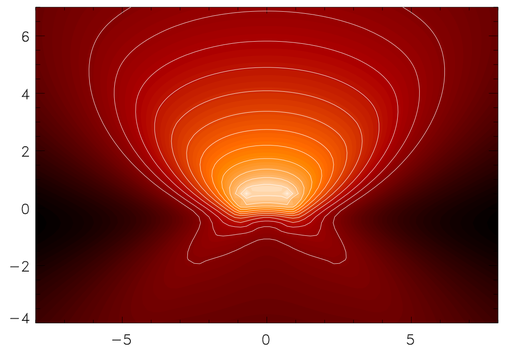

Figure 8: K-band surface brightness of a clumpy torus model for an inclination of 60°. The dynamic range of the contour levels is 2^{12}. The linear scale of the image is in units of the dust sublimation radius (~ 1 pc). The brightest region is the illuminated inner wall on the opposite side of the torus.

To explain the torus substructure in NGC 1068 mentioned above, the existence of cold and dusty clouds in a geometrically thick torus with only a few clouds along the line of sight is required. We have applied the radiative transfer treatment in a clumpy medium (Nenkova et al. 2002, ApJ 570, pp. L9) to our dynamical model of clouds in the torus of NGC 1068. The resulting image (Fig. 8) allows a comparison with the structures (size, shape, and flux) seen in Fig. 6a.